Chem

CellPress

Article

Leaf-Inspired Self-Healing Polymers

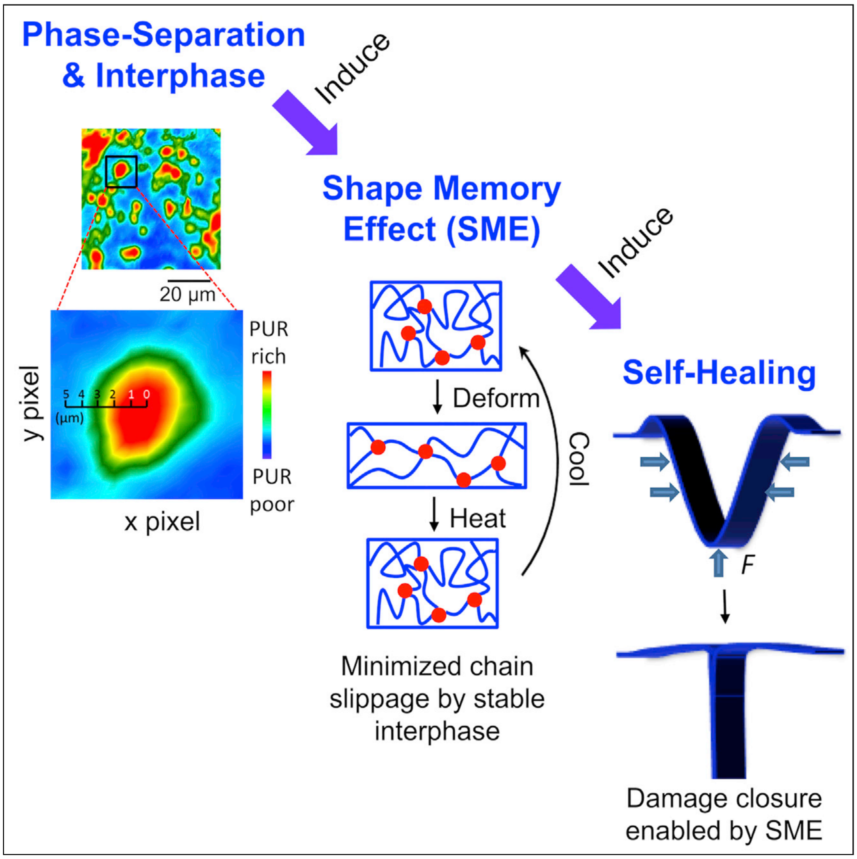

This study demonstrates the role of phase morphology on inducing shape memory effects leading to the self-healing of polymers. Molecular events that occur during this process are established.

Ying Yang, Dmitriy Davydovich,
Chris C. Hornat, Xiaolin Liu,
Marek W. Urban

mareku@clemson.edu

HIGHLIGHTS

Inspired by plants leaves, self-healing fibers are developed

Self-healing occurs as a result of favorable interphase morphologies

Molecular events leading to self-healing are examined by spectroscopic analysis

Correlations between morphology, shape memory, and self-healing are established

Yang et al., Chem 4, 1–9
August 9, 2018 © 2018 Elsevier Inc.
https://doi.org/10.1016/j.chempr.2018.06.001

Please cite this article in press as: Yang et al., Leaf-Inspired Self-Healing Polymers, Chem (2018), https://doi.org/10.1016/j.chempr.2018.06.001

Chem

CellPress

Article

Leaf-Inspired Self-Healing Polymers

Ying Yang,[1] Dmitriy Davydovich,[1] Chris C. Hornat,[1] Xiaolin Liu,[1] and Marek W. Urban[1,2,3,*]

SUMMARY

Hierarchical multiphase fibrous morphologies provide strength and elasticity for biological species, facilitating responses to environmental changes. Wound closure of leaves is one example. If polymers can be formed in a similar manner by introducing multiphase-separated morphologies, self-healing in a variety of commodity materials can be achieved. In these studies, we demonstrate the role of phase morphologies, interphases, and viscoelasticity-driven shape memory effects on self-healing. We synthesized phase-separated polycaprolactone-polyurethane fibrous thermoplastic polymers in which microphase separation facilitates the formation of stable interfacial regions between hard and soft segments. Self-healing can be repeated many times. This behavior is attributed to the shape memory effect, given that micron-scale interphase reduces chain slippage, enabling entropic energy storage during damage. Chemically identical but nanophase-separated copolymers do not exhibit this behavior. These studies show that self-healing can be achieved by morphology control and facilitated by thermal or other volume-induced transitions.

INTRODUCTION

Biological species are able to self-repair repeatedly and autonomously on multiple scale lengths, from DNA macromolecules to larger organs, such as veins, soft or hard tissues, and muscles. Over the last couple of decades, numerous studies have focused on mimicking biological systems to develop self-healing materials. The main motivation behind these efforts is to prolong the lifespan while retaining desired functions of man-made materials. Recent advances in materials capable of self-healing can be classified by a handful of approaches: (1) embedding reactive encapsulated fluids that burst open upon crack propagation to fill and repair damaged areas,[1,2] (2) incorporating reversible covalent and non-covalent bonds into existing structures capable of rebonding after damage,[3–16] (3) physically dispersing superparamagnetic or other nanomaterials that remotely respond to magnetic, electromagnetic, or other energy sources,[17,18] and (4) embedding living organisms capable of re-mending damaged structural features.[19,20] Although these inherently different chemical and physical approaches significantly advanced our understanding of synthetic self-healing materials, biological systems are capable of on-demand self-healing with an incredible degree of efficiency. One example is healing upon mechanical damage of the *Delosperma cooperi* leaves shown in Figure 1A, where wounds can be closed within 60 min by tissue bending or contraction. This response is believed to be due to stored elastic stress built-in within the heterogeneous structure during growth.[21] When the equilibrium is disturbed by mechanical damage the energy will be released, causing viscoelastic shape transformation, bringing the wound edges into contact to heal. Similarly, in mammals, microstructural heterogeneity in cancellous bones is responsible for enhanced shape recovery upon mechanical deformations.[22] Achieving similar functions in real-world polymer-based materials is challenging to say the least.[23]

The Bigger Picture

Developments of self-healing polymers are primarily driven by the desire to prolong materials' lifetime while maintaining their functions. Significant synthetic efforts have been made over the last two decades via the incorporation of dynamic bonds capable of reversible breaking and reforming. However, the role of physical network design in achieving self-healing properties in commodity polymers remains unclear.

Inspired by the self-healing behavior of leaves, we built self-healing into polycaprolactone-polyurethane fibers by controlling morphological features. Favorable viscoelastic properties originating from interphase features facilitate shape memory effects and lead to autonomous damage closure and subsequent self-healing. The creation of morphology-controlled dynamic polymers can be utilized in numerous applications ranging from soft robotics to molecular actuators or morphology-induced information storage to thermomechanical sensing and other devices.

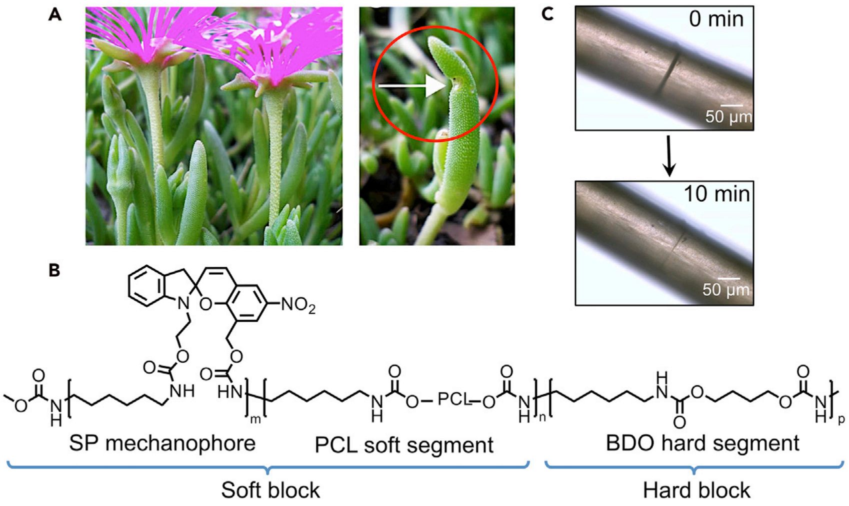

Figure 1. Self-Healing Polycaprolactone-Polyurethane Fibers Inspired by Leaves of Plants

Figure360▷ For a Figure360 author presentation of Figure 1, see http//dx.doi:10.1016/j.chempr.2018.06.001#mmc2.

(A) Succulent plant *Delosperma cooperi* (left) and a leaf showing a healed injury (right, arrow in circled area). Image reprinted from Speck et al.[21] © 2018 Speck et al.; licensee Beilstein-Institut under CC BY 4.0.

(B) Chemical composition of thermoplastic polycaprolactone-polyurethane (PURP) fibers.

(C) Self-healing of PURP fibers upon making a 100-μm deep cut.

Inspired by the role of heterogeneous morphologies in biological systems with built-in stresses, this study explores the role of deliberately introduced phase-separated morphologies that enable energy storage during mechanical damage and viscoelastic shape recovery attributed to built-in shape memory effect (SME) leading to self-healing. Although intuitively SME may potentially contribute to the self-healing of polymers, molecular-level relationships between these events are not obvious and have not been addressed. The early approaches focused on practical applications to improve the self-healing performance of composites by embedding pre-stretched shape memory alloy wires.[24] As the fields of self-healing[25] and shape memory polymers[26–29] evolved independently, shape-memory-assisted self-healing emerged.[30–36] Although practical applications are promising, limited molecular-level mechanisms that would correlate SMEs with damage closure were identified. This study aims to explore how SMEs can facilitate microscale damage closure and identify the role of polymer heterogeneities, if any, in self-healing.

RESULTS AND DISCUSSION

To develop heterogeneities of desirable sizes, we prepared a polymer consisting of well-defined thermoplastic polyurethane copolymerized from polycaprolactone diol (PCL-diol), 1,4-butanediol (BDO), hydroxyl modified spiropyran (SP), and hexamethylene diisocyanate (HDI) drawn into fibers from solution during polymerization (PURP, where PUR stands for polyurethane and P represents that the fibers are produced by cold drawing during polymerization). Whereas polymerization methods are provided in Supplemental Experimental Procedures, Scheme S1, and Figure S1, Figure 1B illustrates PURP copolymer structure. The choice of this copolymer was dictated by the ability of PCL to recrystallize after melting at 65°C and achieve controlled phase-separated morphologies by copolymerizing with BDO and HDI components. As a visual color change indicator of mechanical damage, well-known SP mechanophores were copolymerized into the polymer backbone.[37] Optical images shown in Figure 1C

[1]Department of Materials Science and Engineering, Center for Optical Materials Science Engineering Technologies (COMSET), Clemson University, Clemson, SC 29634, USA

[2]Department of Chemistry, Clemson University, Clemson, SC 29634, USA

[3]Lead Contact

*Correspondence: mareku@clemson.edu

https://doi.org/10.1016/j.chempr.2018.06.001

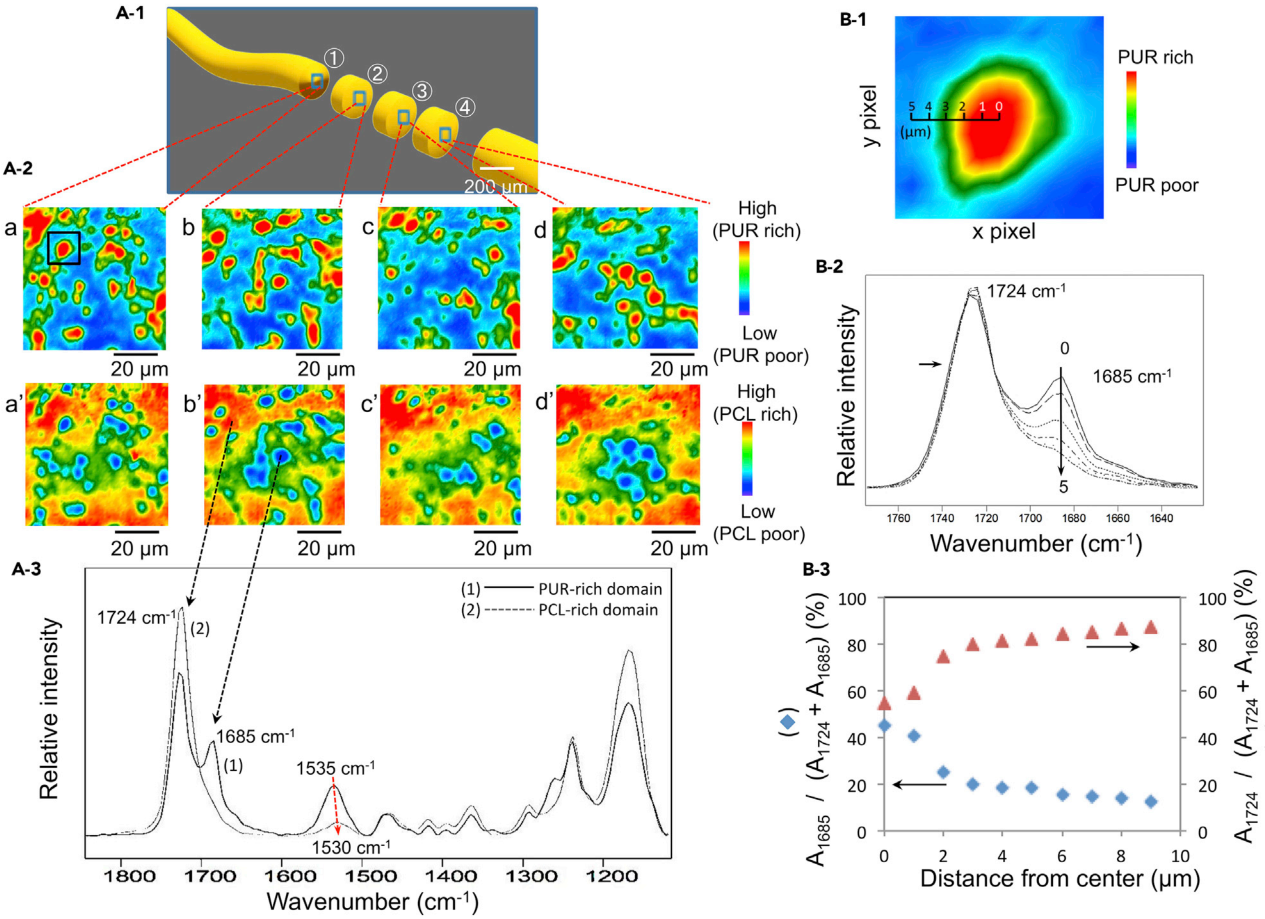

Figure 2. Phase Morphology of PURP Polymers Showing Micron-Scale Phase Separation along with Gradient Interphase

Figure360▷ For a Figure360 author presentation of Figure 2, see http//dx.doi:10.1016/j.chempr.2018.06.001#mmc2.

(A-1) Schematic representation of PURP cross-section of a 200-μm thick fiber.

(A-2) IR images of the 1,685 cm^{-1} (a–d) and 1,724 cm^{-1} (a′–d′) bands due to PUR and PCL C=O vibrations, respectively, collected from the cross-sections 1–4 marked as the squares in (A-1) for PURP fiber.

(A-3) Corresponding IR spectra recorded from PUR-rich (blue in a′–d′) and PCL-rich (red in a′–d′) domains indicated by the black arrows. The red arrow indicates that the amide II band shifted from 1,535 cm^{-1} for the PUR-rich doamin to 1,530 cm^{-1} for the PCL-rich domain.

(B-1) IR image of the 1,685 cm^{-1} band enlarged on a PUR-rich domain (marked by the square in A-2a).

(B-2) IR spectra of carbonyl regions, where traces 0–5 were collected from the corresponding areas shown in (B-1) marked by 0–5, respectively.

(B-3) Percentage of the 1,724 cm^{-1} (ester C=O) and 1,685 cm^{-1} (urethane C=O) band areas (A_{1724} and A_{1685}) within 1,780–1,640 cm^{-1} region plotted as a function of the distance from the center of PUR-rich domain shown in (B-1) (0–9 μm). The percentage is calculated on the basis of integrated areas of the deconvoluted bands.

illustrate that when a PURP fiber is damaged, a 100-μm-deep cut vanishes within 10 min upon exposure slightly above melting transition of PCL (T_m = 65°C).

Figure 2A-1 shows four 100-μm-thick cross-sections of PURP fibers. As seen, each sliced cross-section exhibits micron-size phase separation demonstrated by infrared (IR) images of urethane groups shown in Figure 2A-2, a–d. The micron-size PUR-rich domains (red) are formed within a PUR-deficient matrix (blue). The corresponding PCL distribution is detected upon tuning to the PCL ester linkages (Figure 2A-2, a′–d′), where the PCL segments are mainly distributed within the matrix (red and yellow regions). Similar morphologies are detected along the longitudinal direction of individual fibers. Chemical analysis of PUR- and PCL-rich domains shown in Figure 2A-3 illustrates the carbonyl and amide II band intensity differences of the two domains. Another feature shown in Figures 2B-1 and 2B-2 is a gradual decrease of the urethane content (1,685 cm^{-1}) when going from the center of PUR-rich domain outward toward the PCL-rich domain in 1-μm increments (0 ⇒ 5). Figure 2B-3 plots relative intensities of urethane and ester C=O groups as a function of the distance from the PUR-rich center. These results show the presence of micron-scale interphase between the two domains. The phase separation is also confirmed by differential scanning calorimetry measurements with two melting transitions (T_m) at 51°C and 168°C due to PCL- and PUR-rich domains, respectively (Figure S2).

To achieve nanoscale phase separation, we applied a melt-drawn process to chemically identical polymers (Scheme S1). Designated as PURM (where PUR stands for polyurethane and M stands for the melt-drawing method), nanoscale phase separation becomes indistinguishable in IR imaging (Figure S3; IR imaging spatial resolution ~1 μm), but the presence of two melting points (T_m) at 51°C and 162°C (Figure S2) along with atomic force microscopy phase images (Figure S3) indicate nanoscale phase separation. Although a 6°C lower T_m signifies smaller-size crystals of the hard segments, in contrast to microphase-separated PURPs, nanoscale phase-separated PURM fibers virtually do not self-heal within the same time frame. As seen in Figure 3A-1, a cut in the microphase-separated PURP (t = 0 min) closes within 10 min. After damage, tensile strain and stress at break plotted as a function of healing time shown in Figure 3A-2 illustrate that compared with the undamaged state with the strain of 1,015% and stress at 29.2 MPa, upon self-healing, 35.8% and 52.5% of the original strain and stress is recovered within first 10 min, to reach 82.6% and 87.0% after 120 min. Parallel experiments conducted on nanophase-separated PURM fibers are shown in Figures 3B-1 and 3B-2. The ultimate strain and stress of undamaged PURM are 1,090% and 34.3 MPa, respectively, and after 120 min the recovery reaches only ~48% of the original strain and ~51% of the original tenacity (note that these values for tensile stress and strain at break represent an average of six measurements [for standard deviation, see Table S1]; the plots shown in Figures 3A-2 and 3B-2 represent an example of one measurement). Notably, at the healing temperature, PURP and PURM maintain elasticity within the rubbery plateau regions (dynamic mechanical analysis [DMA]; Figure S4).

Since the microphase-separated PURPs exhibit ~35% higher self-healing efficiency, the question is why chemically identical polymers with the same molecular weight, but different domain sizes and degrees of heterogeneity, exhibit entirely different self-healing characteristics. Considering viscoelastic and recently quantified entropic contributions to SME in synthetic polymers,[38] thermomechanical shape memory cycles (SMCs) were conducted in which a "cold" programming cycle was employed to determine the SME on self-healing under the same conditions. As shown in Figure 3C, microphase-separated (PURP) and nanophase-separated (PURM) fibers were uniaxially deformed to 200% strain (ε_{max}) at room temperature (23°C), which is below their melting transitions, and at a strain rate of 100%/min. Upon load removal, microphase-separated (PURP) and nanophase-separated (PURM) fibers contracted to 126% and 147% strains (ε_f), respectively, with fixity ratios ($R_{f=}\, \varepsilon_f/\varepsilon_{max}$) of 63.0% and 73.5%, respectively. When the temperature was increased to 65°C, shape recovery was initiated, and the residual strains detected after recovery (ε_r) were 43% and 85%, respectively. At the same time, the shape recovery ratios ($R_r = (\varepsilon_{max} - \varepsilon_r)/\varepsilon_{max}$) were 78.5% and 57.5%, respectively. These bulk measurements clearly suggest a relationship between the degree of phase separation and shape recovery. For comparison, standard thermomechanical SMCs of PURP and PURM are provided in Figure S5.

To identify molecular processes responsible for SME, we conducted X-ray diffraction (XRD) and Fourier transform IR analysis. Figure 3Di plots the percentage of

Please cite this article in press as: Yang et al., Leaf-Inspired Self-Healing Polymers, Chem (2018), https://doi.org/10.1016/j.chempr.2018.06.001

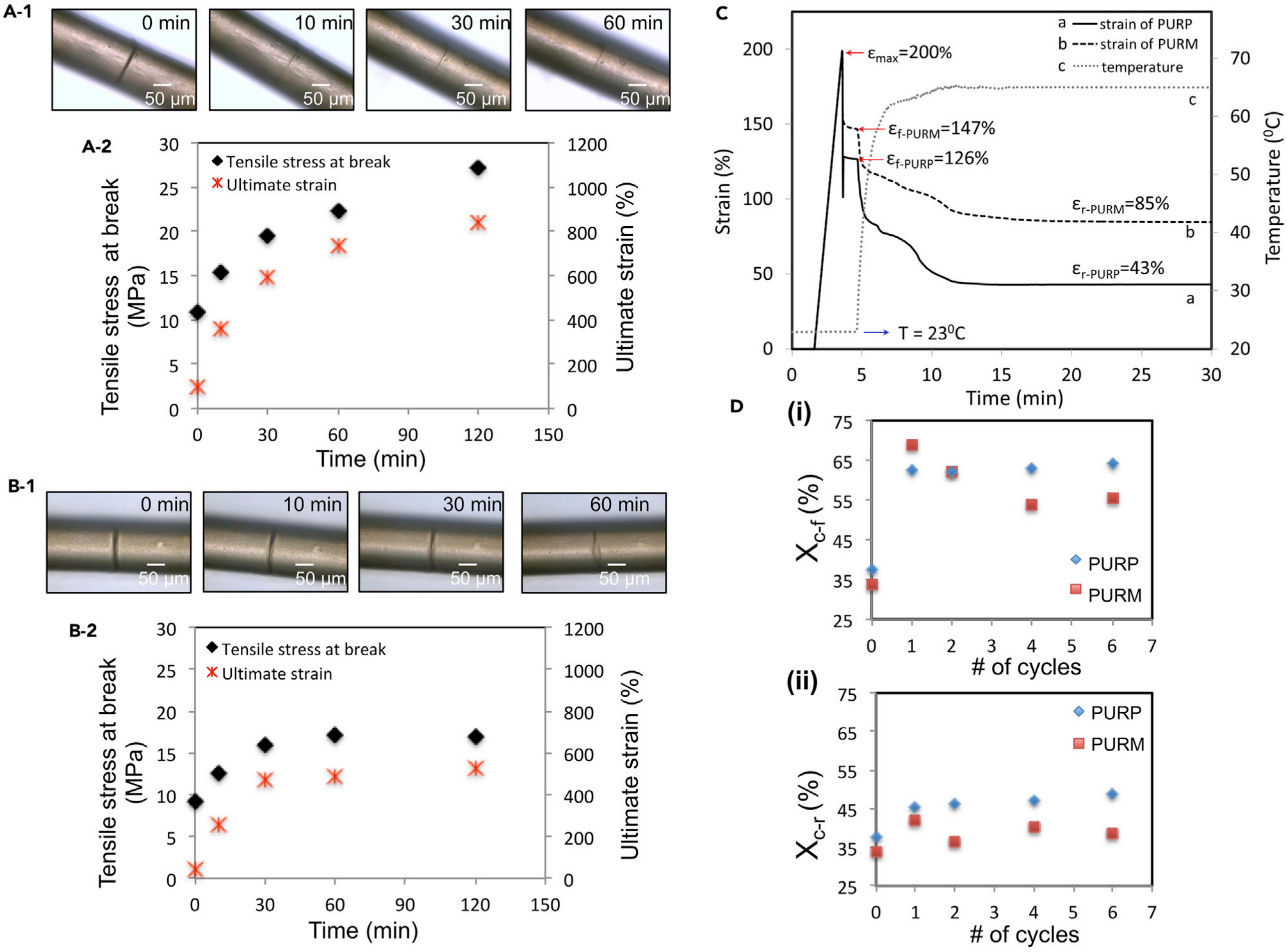

Figure 3. Self-Healing and Shape Memory Properties of PURP and PURM Fibers

(A-1) Optical images of self-healable microphase-separated PURP fibers.

(A-2) Tensile stress and strain at break are plotted as a function of self-healing time for PURP fibers. The dimensions of the scratch are 8 × 50 μm (width × depth), and self-healing was conducted at 65°C.

(B-1) Optical images of self-healing for nano-phase-separated (PURM) fibers.

(B-2) tensile stress and strain at break are plotted as a function of self-healing time for PURM fibers. The dimensions of the scratch are 8 × 50 μm (width × depth), and self-healing was conducted at 65°C.

(C) Thermomechanical SMCs of PURP and PURM polymers.

(D) The degree of crystallinity in deformed (i) and shape-recovered (ii) states for six consecutive SMCs; χ_{c-f} is the percentage of crystallinity at unload strain, and χ_{c-r} is the same after shape recovery.

crystallinity (χ_c) for microphase- and nanophase-separated fibers at unload strain (ε_f) for six consecutive SMCs (% χ_{c-f}) (XRD reference data are provided in Figure S6). The strain-induced crystallinity increases by ~30% after the first SMC, but for the remaining cycles only a slight %χ_{c-f} increase for microphase-separated fiber is detected. In contrast, the %χ_{c-f} in nanophase-separated fiber initially increases and then decreases after first four cycles and levels off. The percentage of crystallinity after shape recovery (% χ_{c-r}) plotted in Figure 3Dii shows ~8% increase after the first SMC for microphase-separated (PURP) and nanophase-separated (PURM) fibers, which is attributed to the residual strain (Figure 3C). After six SMCs, % χ_{c-f} and % χ_{c-r} values are lower in PURM than in PURP. Our hypothesis for this behavior is that chain slippage of urethane segments from PUR-rich to PCL-rich domains occurs during deformation of PURM, thus inhibiting PCL chain packing. On the contrary, the

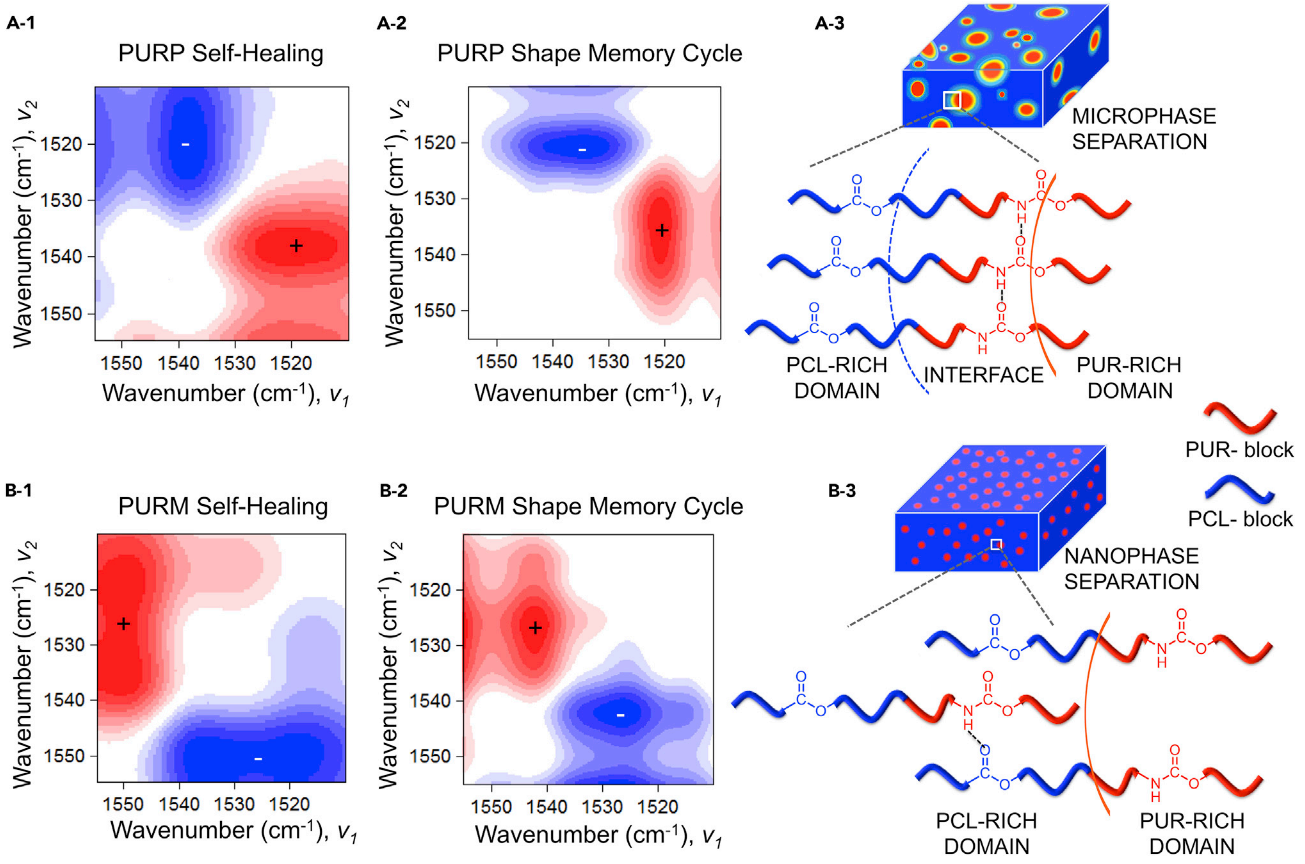

Figure 4. 2D-FTIR Analysis Identifying Molecular Events during Self-Healing and Shape Memory Cycles

Asynchronous 2D-FTIR correlation spectra of (A-1) PURP before and after self-healing, (A-2) PURP before and after the first SMC, (B-1) PURM before and after self-healing, and (B-2) PURM before and after the first SMC zoomed in to the 1,555–1,510 cm^{-1} range. The 2D-FTIR spectra were calculated with no reference and provide information on the bands' relative intensity changes. ν_1 corresponds to the IR spectra of the original material before damage or deformation, and ν_2 corresponds to spectra collected after perturbation such as self-healing or SMC. Schematic illustrations of molecular events in micro- and nanophase-separated PURP and PURM copolymers upon self-healing are shown in (A-3) and (B-3), respectively.

distribution of PUR-rich and PCL-rich domains in microphase-separated PURP remains less disturbed. These conclusions are also supported by IR imaging analysis of microphase-separated PURP cross-sections after deformation (at unloading strain) as well as after the SMCs (Figure S7). The microscale phase-separated interfacial regions may act as stable junction points inhibiting chain slippage during mechanical deformation.

To examine this hypothesis and further substantiate whether the same phenomenon governs SME and self-healing, we utilized 2D-FTIR correlation spectroscopy. Figures 4A-1 and 4B-1 show the results of asynchronous 2D-FTIR correlation of molecular vibrations that are affected by the damage-repair cycle in microphase- and nanophase-separated copolymers, respectively. For microphase separate PURPs, two antisymmetric crosspeaks along the diagonal lines are detected, indicating two types of H bonding: urethane-urethane (1,536 cm^{-1}) and urethane-ester (PCL) (1,521 cm^{-1}). Detailed 2D-FTIR analysis is provided in the Supplemental Experimental Procedures and Figures S8–S12. The presence of the positive crosspeak (Figure 4A-1) after self-healing is attributed to the increased urethane-urethane H bonding with respect to urethane-ester counterpart. In contrast, an opposite trend is observed for PURM. The negative intensity shown in Figure 4B-1 after the

Please cite this article in press as: Yang et al., Leaf-Inspired Self-Healing Polymers, Chem (2018), https://doi.org/10.1016/j.chempr.2018.06.001

damage-repair cycle indicates the decrease of urethane-urethane H bonding with respect to the urethane-ester. If the damage-repair cycle is attributed to the SME, the same spectroscopic responses are expected after the first SMC. Indeed, Figures 4A-2 and 4B-2 illustrate asynchronous 2D-FTIR correlation before and after one SMC and clearly show that the same responses are detected for PURP and PURM. Thus, a micron-scale damage-repair cycle and macroscopic shape memory recovery are governed by the same molecular events: the increase of urethane-urethane H bonding in microphase-separated PURP copolymers and further phase separation at the healing temperatures as the two phases are immiscible. On the other hand, the increase of urethane-ester interactions in nanophase-separated PURM indicates that PUR blocks are partially dispersed in PCL-rich domains after SMC and self-healing, thus indicating that nanosize hard-segment crystals resulting from urethane-urethane H bonding dissociate during deformation. Further support for the dissociation of H bonding as well as the % χ_c decrease after mechanical damage for microphase- and nanophase-separated fibers is provided in Figures S12–S14. The analysis of junction densities due to hard segments and chain entanglements after the first shape memory cycle shows that for microphase-separated PURP, there is virtually no change (0.68–0.65 kmol/m^3, corresponding to the molecular weight between junction points from 1.68 to 1.75 kDa). In contrast, the junction density in nanophase-separated PURM is reduced over 3-fold from 1.8 to 0.46 kmol/m^3, also reflected in the increase of the molecular weight between the junction points from 0.63 to 2.5 kDa (determined from the rubbery plateau moduli of DMA curves; Figure S4). These results along with 2D FTIR and XRD provide further evidence that microphase-separated PUR-rich domains along with gradually changing PUR-to-PCL microscale interphase have a stabilizing effect by reducing the degree of chain slippage during thermomechanical SMC, thus allowing entropic energy storage during damage, which is responsible for shape recovery. On the other hand, plastic deformations associated with the dissociations of hard-segment crystalline domains lead to lower shape recovery ratios in nanoscale phase-separated PURMs.

On the basis of these results, the following mechanism of wound closure is proposed. For a microphase-separated system (Figure 4A-3), a PUR-rich domain and the microscale interphase inhibits PUR blocks from disengagement under mechanical forces. As a result, PCL-rich domains are able to store entropic energy, whereby the crystalline blocks unfold and low T_g amorphous segments elongate, thus reducing entropy. However, when temperature is raised and the chains in the PCL-rich domain gain sufficient mobility, they return to the randomized state to maximize entropy. The stored energy is released and shape recovery occurs, which is responsible for damage closure in microphase-separated polymers. This is schematically depicted in Figure 4A-3. During this process, localized chain diffusion, recrystallization of PCL chains, and reformation of H bonds localized within the damaged interface occur, resulting in self-healing. On the contrary, for nanophase-separated copolymers depicted in Figure 4B-3, the disengagement of PUR blocks from PUR-rich domains and slippage into a PCL-rich phase upon mechanical deformation leads to energy dissipation during deformation. As a result, shape recovery and wound closure do not occur to the same extent. Thus, built-in controllable heterogeneities at different physical length scales of chemically identical components may facilitate entropy storage that leads to self-healing via SME. Additional evidence that the role of heterogeneities in self-healing is demonstrated by varying the PUR-rich domain sizes in microphase PURPs by changing the content of PUR hard segments (Table S1 and Figure S15), which compromises self-healing efficiency. Reversible color changes during the damage-repair cycle can be induced as a result of the presence of spiropyran incorporated into the polymer backbone (Figure S16).

Conclusion

In summary, felicitous heterogeneities intentionally induced in polymers enable elastic energy storage during damage, which can be recovered during self-healing. These studies identified the relationship between the SMEs and self-healing in microphase-separated polymers whereby the ability of polymer networks to minimize plastic deformation and store entropic energy during deformation is responsible for shape recovery, thus facilitating damage closure. The presence of phase-separated microdomains with stabilizing interfacial regions serve as an energy reservoir, facilitating polymer recovery upon mechanical damage without elaborate chemical modifications. The damage-repair cycle can be repeated many times while retaining mechanical properties, thus enhancing the material's sustainability. Although it is well known that embedding rigid nano-objects usually enhances physical properties, introducing stabile interfacial regions facilitating energy storage during mechanical damage offers alternative approaches for the development of self-healable commodity polymers without chemical modification.

EXPERIMENTAL PROCEDURES

Detailed synthesis and characterization procedures are provided in the Supplemental Information.

SUPPLEMENTAL INFORMATION

Supplemental Information includes Supplemental Experimental Procedures, 16 figures, 1 table, and 1 scheme and can be found with this article online at https://doi.org/10.1016/j.chempr.2018.06.001.

ACKNOWLEDGMENTS

This work was supported in part by the Established Program to Stimulate Competitive Research under National Science Foundation award OIA-1655740, the Division of Materials Research program under award DMR1744306, and the J.E. Sirrine Foundation Endowment at Clemson University.

AUTHOR CONTRIBUTIONS

Conceptualization, Y.Y. and M.W.U.; Methodology, Y.Y. and M.W.U.; Investigation, Y.Y., D.D., C.C.H., and X.L.; Writing – Original Draft, Y.Y. and M.W.U; Writing – Review & Editing, Y.Y. and M.W.U.; Supervision. M.W.U.; Funding Acquisition, M.W.U.

DECLARATION OF INTERESTS

The authors declare no competing financial interests.

Received: January 11, 2018
Revised: March 28, 2018
Accepted: May 31, 2018
Published: June 28, 2018

REFERENCES AND NOTES

1. White, S.R., Sottos, N.R., Geubelle, P.H., Moore, J.S., Kessler, M.R., Sriram, S.R., Brown, E.N., and Viswanathan, S. (2001). Autonomic healing of polymer composites. Nature *409*, 794–797.
2. Toohey, K.S., Sottos, N.R., Lewis, J.A., Moore, J.S., and White, S.R. (2007). Self-healing materials with microvascular networks. Nat. Mater. *6*, 581–585.
3. Chen, X., Dam, M.A., Ono, K., Mal, A., Shen, H., Nutt, S.R., Sheran, K., and Wudl, F. (2002). A thermally re-mendable cross-linked polymeric material. Science *295*, 1698–1702.
4. Ghosh, B., and Urban, M.W. (2009). Self-repairing oxetane-substituted chitosan polyurethane networks. Science *323*, 1458–1460.
5. Imato, K., Nishihara, M., Kanehara, T., Amamoto, Y., Takahara, A., and Otsuka, H. (2012). Self-healing of chemical gels

Please cite this article in press as: Yang et al., Leaf-Inspired Self-Healing Polymers, Chem (2018), https://doi.org/10.1016/j.chempr.2018.06.001

cross-linked by diarylbibenzofuranone-based trigger-free dynamic covalent bonds at room temperature. Angew. Chem. Int. Ed. *51*, 1138–1142.

6. Ying, H., Zhang, Y., and Cheng, J. (2014). Dynamic urea bond for the design of reversible and self-healing polymers. Nat. Commun. *5*, 3218.
7. Sijbesma, R.P., Beijer, F.H., Brunsveld, L., Folmer, B.J., Hirschberg, J.K., Lange, R.F., Lowe, J.K., and Meijer, E. (1997). Reversible polymers formed from self-complementary monomers using quadruple hydrogen bonding. Science *278*, 1601–1604.
8. Kalista, S.J., Jr., Ward, T.C., and Oyetunji, Z. (2007). Self-healing of poly (ethylene-co-methacrylic acid) copolymers following projectile puncture. Mech. Adv. Mater. Struct. *14*, 391–397.
9. Cordier, P., Tournilhac, F., Soulié-Ziakovic, C., and Leibler, L. (2008). Self-healing and thermoreversible rubber from supramolecular assembly. Nature *451*, 977–980.
10. Burnworth, M., Tang, L., Kumpfer, J.R., Duncan, A.J., Beyer, F.L., Fiore, G.L., Rowan, S.J., and Weder, C. (2011). Optically healable supramolecular polymers. Nature *472*, 334–337.
11. Holten-Andersen, N., Harrington, M.J., Birkedal, H., Lee, B.P., Messersmith, P.B., Lee, K.Y.C., and Waite, J.H. (2011). pH-induced metal-ligand cross-links inspired by mussel yield self-healing polymer networks with near-covalent elastic moduli. Proc. Natl. Acad. Sci. USA *108*, 2651–2655.
12. Nakahata, M., Takashima, Y., Yamaguchi, H., and Harada, A. (2011). Redox-responsive self-healing materials formed from host–guest polymers. Nat. Commun. *2*, 511.
13. Chen, Y., Kushner, A.M., Williams, G.A., and Guan, Z. (2012). Multiphase design of autonomic self-healing thermoplastic elastomers. Nat. Chem. *4*, 467–472.
14. Yang, Y., and Urban, M.W. (2014). Self-repairable polyurethane networks by atmospheric carbon dioxide and water. Angew. Chem. Int. Ed. *53*, 12142–12147.
15. Li, C.-H., Wang, C., Keplinger, C., Zuo, J.-L., Jin, L., Sun, Y., Zheng, P., Cao, Y., Lissel, F., Linder, C., et al. (2016). A highly stretchable autonomous self-healing elastomer. Nat. Chem. *8*, 618–624.
16. Yang, Y., and Urban, M.W. (2017). Self-healing of glucose-modified polyurethane networks facilitated by damage-induced primary amines. Polym. Chem. *8*, 303–309.
17. Corten, C.C., and Urban, M.W. (2009). Repairing polymers using oscillating magnetic field. Adv. Mater. *21*, 5011–5015.
18. Huang, L., Yi, N., Wu, Y., Zhang, Y., Zhang, Q., Huang, Y., Ma, Y., and Chen, Y. (2013). Multichannel and repeatable self-healing of mechanical enhanced graphene-thermoplastic polyurethane composites. Adv. Mater. *25*, 2224–2228.
19. Jonkers, H.M., Thijssen, A., Muyzer, G., Copuroglu, O., and Schlangen, E. (2010). Application of bacteria as self-healing agent for the development of sustainable concrete. Ecol. Eng. *36*, 230–235.
20. Wang, J., Soens, H., Verstraete, W., and De Belie, N. (2014). Self-healing concrete by use of microencapsulated bacterial spores. Cem. Concr. Res. *56*, 139–152.
21. Speck, O., Schlechtecdahl, M., Borm, F., Kampowski, T., and Speck, T. (2018). Humidity-dependent wound sealing in succulent leaves of *Delosperma cooperi*—an adaptation to seasonal drought stress. Beilstein J. Nanotechnol. *9*, 175–186.
22. Torres, A.M., Matheny, J.B., Keaveny, T.M., Taylor, D., Rimnac, C.M., and Hernandez, C.J. (2016). Material heterogeneity in cancellous bone promotes deformation recovery after mechanical failure. Proc. Natl. Acad. Sci. USA *113*, 2892–2897.
23. Patrick, J.F., Robb, M.J., Sottos, N.R., Moore, J.S., and White, S.R. (2016). Polymers with autonomous life-cycle control. Nature *540*, 363–370.
24. Kirkby, E.L., Rule, J.D., Michaud, V.J., Sottos, N.R., White, S.R., and Månson, J.A.E. (2008). Embedded shape-memory alloy wires for improved performance of self-healing polymers. Adv. Funct. Mater. *18*, 2253–2260.
25. Yang, Y., and Urban, M.W. (2013). Self-healing polymeric materials. Chem. Soc. Rev. *42*, 7446–7467.
26. Lendlein, A., and Langer, R. (2002). Biodegradable, elastic shape-memory polymers for potential biomedical applications. Science *296*, 1673–1676.
27. Xie, T. (2010). Tunable polymer multi-shape memory effect. Nature *464*, 267.
28. Liu, C., Qin, H., and Mather, P. (2007). Review of progress in shape-memory polymers. J. Mater. Chem. *17*, 1543–1558.
29. Zhao, Q., Qi, H.J., and Xie, T. (2015). Recent progress in shape memory polymer: new behavior, enabling materials, and mechanistic understanding. Prog. Polym. Sci. *49*, 79–120.
30. Nji, J., and Li, G. (2010). A biomimic shape memory polymer based self-healing particulate composite. Polymer *51*, 6021–6029.
31. Rodriguez, E.D., Luo, X., and Mather, P.T. (2011). Linear/network poly (ε-caprolactone) blends exhibiting shape memory assisted self-healing (SMASH). ACS Appl. Mater. Interfaces *3*, 152–161.
32. Heo, Y., and Sodano, H.A. (2014). Self-healing polyurethanes with shape recovery. Adv. Funct. Mater. *24*, 5261–5268.
33. Rivero, G., Nguyen, L.-T.T., Hillewaere, X.K., and Du Prez, F.E. (2014). One-pot thermo-remendable shape memory polyurethanes. Macromolecules *47*, 2010–2018.
34. Ur Rehman, H., Chen, Y., Hedenqvist, M.S., Li, H., Xue, W., Guo, Y., Guo, Y., Duan, H., and Liu, H. (2018). Self-healing shape memory PUPCL copolymer with high cycle life. Adv. Funct. Mater. *28*, 1704109.
35. Miyamae, K., Nakahata, M., Takashima, Y., and Harada, A. (2015). Self-healing, expansion-contraction, and shape-memory properties of a preorganized supramolecular hydrogel through host-guest interactions. Angew. Chem. Int. Ed. *54*, 8984–8987.
36. Fang, Z., Zheng, N., Zhao, Q., and Xie, T. (2017). Healable, reconfigurable, reprocessable thermoset shape memory polymer with highly tunable topological rearrangement kinetics. ACS Appl. Mater. Interfaces *9*, 22077–22082.
37. Davis, D.A., Hamilton, A., Yang, J., Cremar, L.D., Van Gough, D., Potisek, S.L., Ong, M.T., Braun, P.V., Martínez, T.J., and White, S.R. (2009). Force-induced activation of covalent bonds in mechanoresponsive polymeric materials. Nature *459*, 68–72.
38. Hornat, C.C., Yang, Y., and Urban, M.W. (2016). Quantitative predictions of shape-memory effects in polymers. Adv. Mater. *29*, 1603334.